Geophysical Journal International

Geophys. J. Int. (2012) **191,** 557–568 doi: 10.1111/j.1365-246X.2012.05649.x

Precise analysis of ICESat altimetry data and assessment of the hydrostatic equilibrium for subglacial Lake Vostok, East Antarctica

H. Ewert,[1] S. V. Popov,[2] A. Richter,[1] J. Schwabe,[1] M. Scheinert[1] and R. Dietrich[1]

[1] *Technische Universität Dresden, Institut für Planetare Geodäsie,* 01062 *Dresden, Germany. E-mail: Heiko.Ewert@tu-dresden.de*
[2] *Polar Marine Geosurvey Expedition,* 24 *Pobeda Street, Lomonosov,* 188512 *St Petersburg, Russia*

Accepted 2012 August 14. Received 2012 June 20; in original form 2012 April 25

SUMMARY

Based on the Ice, Cloud and Land Elevation Satellite (ICESat) laser altimetry data, the hydrostatic equilibrium (HE) condition for the subglacial Lake Vostok, East Antarctica, is evaluated. A digital elevation model (DEM) of the ice surface is derived by a regional crossover adjustment. The analysis of the DEM and its comparison with GPS derived ice-surface elevations and an ice-surface DEM based on radar altimetry data reveal an overall accuracy of better than ± 0.7 m for the lake area. The DEM is combined with an ice-thickness model and a regional geoid model to determine the deviation of the local ice-surface height from HE. For large parts of the lake, the ice sheet fulfils the HE. Our results reveal a strong positive deviation of about 10 m along the lake shoreline. In addition, positive deviations are found in the northern part of the lake which coincide with ice rumples detected by radio-echo sounding. In the southern part of the lake, we find a linear negative deviation (-4.0 m) which coincides with the convoy route from Vostok station to Mirny base. In addition to the DEM, relative biases for the ICESat laser operational periods are determined in the regional crossover adjustment.

Key words: Satellite geodesy; Satellite gravity; Glaciology; Antarctica.

1 INTRODUCTION

Lake Vostok, located in East Antarctica (Fig. 1), is the largest of the subglacial lakes discovered to date (Popov & Masolov 2007; Siegert *et al.* 2007). Since the confirmation of their existence (Kapitsa *et al.* 1996; Siegert *et al.* 2000), subglacial lakes have been in the focus of multidisciplinary scientific interest (Karl *et al.* 1999; Petit *et al.* 1999; Priscu *et al.* 1999; Bell *et al.* 2002). Lake Vostok plays an outstanding role among them, supported furthermore by the recent progress of the drilling activities in its southern part. To understand its origin, extent and influence on ice flow, numerous geophysical and glaciological investigations have been carried out in the Lake Vostok area during the last two decades (Siegert *et al.* 2011). An important question for many of these investigations is to which extent the ice sheet over the lake fulfils the hydrostatic equilibrium (HE).

The data obtained by ground based radio-echo sounding (RES, Popov *et al.* 2006; Masolov *et al.* 2006) in the Lake Vostok area since 1998 has been used to infer the thickness of the ice sheet and to locate the grounding line limiting the lake. This data set is complemented by airborne geophysical data (Studinger *et al.* 2003). Wendt *et al.* (2005) provided the observational evidence on small elevation variations of the ice-sheet surface in the lake area induced by tides and air pressure forcing. Both processes produce ice-surface height variations in space and time with in the order of 1 cm. The synthetic aperture radar (SAR) interferograms (Wendt *et al.* 2005, figs 8 and 9) showing the vertical displacement of the floating ice relative to the grounded ice sheet provided also insights into the location of the lake shore, islands and peninsulas, which partly were later confirmed by RES (Popov *et al.* 2006). Combined geodetic, geophysical and glaciological *in situ* measurements were used by Richter *et al.* (2008) to investigate the elevation change of the ice surface between 2001/2002 and 2006/2007 as well as the local ice-mass balance in the area of Vostok station. Thereby, the fundamental assumption was made that the ice sheet above Lake Vostok is in HE. In addition, recent investigations based on numerical modelling (Williams 2001; Pattyn *et al.* 2004; Thoma *et al.* 2008) attempted to quantify various processes at the water-ice interface.

A precise knowledge of the geometry of the surface of the ice sheet covering the lake is a fundamental prerequisite for geophysical, glaciological, climatological and related investigations. Rémy *et al.* (1999), Roemer *et al.* (2007) and Studinger *et al.* (2003) generated and investigated digital elevation models (DEM) of the ice-sheet surface using satellite radar (ERS-1) and airborne laser altimetry data.

In this work, we combine a new ice-surface DEM with an ice-thickness model based on RES and a geoid model to quantitatively verify the state of HE of the ice sheet over Lake Vostok. The Ice, Cloud and Land Elevation Satellite (ICESat) mission provided a novel data set for the inference of regional ice-surface DEMs. For the determination of the DEM introduced in the evaluation of the

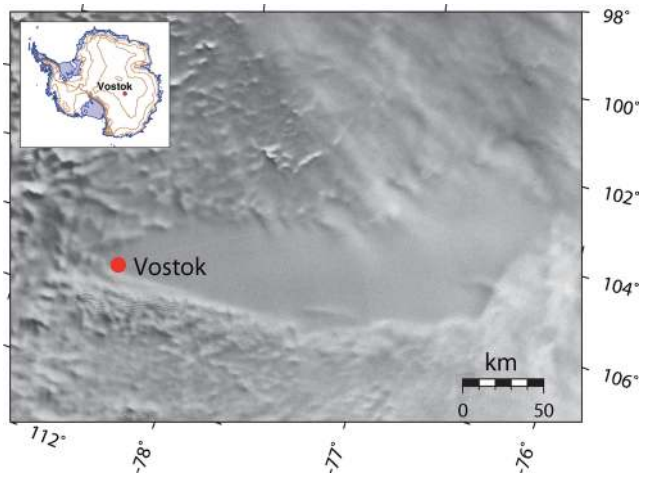

Figure 1. Lake Vostok area in a SAR image from the RADARSAT-1 satellite mission (Jezek & RAMP product team 2002). The subglacial lake is manifested by a very flat and smooth ice surface. The Russian antarctic research station Vostok is located in the southern part of the lake area.

HE, a regional crossover analysis is performed on the complete set of ICESat laser altimetry data obtained in the Lake Vostok area. It yields, in addition to the DEM, also relative estimates of elevation biases for the individual laser operational periods (LOP, Urban & Schutz 2005; Gunter *et al.* 2009).

2 ICESAT-DEM OF THE ICE SURFACE

2.1 Data analysis and methodology

The ICESat mission was launched in 2003 January as a part of NASA's Earth Observing System of satellites and ended in 2010 February (Schutz *et al.* 2005). With an orbital inclination of 94°, this altimetry mission was particularly well suited to observe the interannual and long-term elevation changes of the Greenland and Antarctic ice sheets (Zwally *et al.* 2002). The Geoscience Laser Altimeter System (GLAS) comprised three independent lasers which worked on two different frequencies. For the altimetry measurements, the laser produced a 1064 nm wavelength pulse (Zwally *et al.* 2002; Abshire *et al.* 2005). The diameter of the footprint varies between 60 and 70 m. Successive footprints are separated by about 172 m (Abshire *et al.* 2005). Therefore, ICESat provides time-series of surface elevations of the Earth with an unprecedented along-track resolution (Luthcke *et al.* 2005). Due to a strong energy degradation of the emitted laser pulse, discovered during the validation and calibration phase, the mission was changed from continuous measurements to a measurement of 33-d operation periods two to three times per year (Abshire *et al.* 2005; Schutz *et al.* 2005). A detailed overview of the ICESat mission was given by Zwally *et al.* (2002) and Schutz *et al.* (2005).

For our investigation, we used the GLAS 12 data product in release 531 (NSIDC 2011) containing the measurements over the Greenland and Antarctic ice sheets. The data set covers the time span from 2003 February to 2009 October, corresponding to the LOP 1A–2F. Fig. 2 shows the spatial distribution of the ascending and descending elevation profiles over the Lake Vostok area. The across-track spacing in this area varies between 10 and 20 km.

In a first step, the elevation profiles were screened to exclude outliers. We utilized the quality flags and auxiliary information given within the data set itself (NSIDC 2011). In this way, all measurements were removed for which more than one peak was found in the return echo. A 'pseudo-cloud filter' as described by Nguyen & Herring (2005) was applied removing all measurements with a receiver gain value exceeding 100 counts. The 'attitude-offnadir-flag' was applied to exclude elevation profiles recorded during off-nadir operations. At the beginning of the ICESat mission, saturated waveforms led to biased elevations (Fricker *et al.* 2005). We therefore applied the saturation range correction provided together with the GLAS 12 data product since release 428. In addition, we applied all tidal corrections given by the standard models which were used for the ICESat data processing.

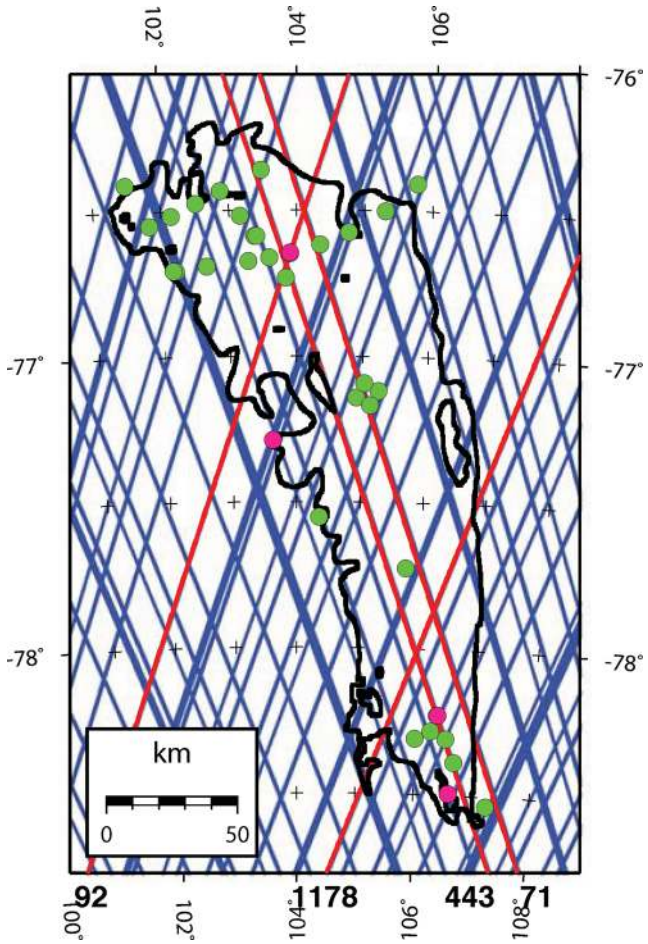

Figure 2. ICESat data coverage in the Lake Vostok area. The elevation profiles are shown in blue and red. Red profiles are analysed in more detail (see text), their reference track numbers are indicated below the map. Green and pink dots show the location of GPS sites. Pink dots denote GPS sites which have a distance shorter than 80 m to the closest ICESat footprint. The shoreline (black) was derived from terrestrial radio-echo sounding (Popov & Masolov 2007; Popov & Chernoglazov 2011).

Particular attention has to be payed to the elevation biases between the individual LOPs (Gunter *et al.* 2009). In this study, we use a regional crossover adjustment (RCA) method to account for biases between the elevation profiles. These biases can be treated in the same way as radial orbit errors.

Since the beginning of the satellite altimetry era, the RCA has been a common tool to reduce the influence of radial orbit errors (Schrama 1989; Gysen & Coleman 1997; Rummel & Sansò 1993). In the case that only radial errors are considered and the RCA is performed for a relatively small area a non-dynamic RCA can be used to adjust the biased altimetry data. The intersection point of

an ascending (index i) and a descending (j) elevation profile is defined as a crossover. The crossover difference is then the difference of the elevations interpolated from both elevation profiles to the intersection point

$$\Delta h_{ij} = H_j - H_i, \tag{1}$$

where Δh_{ij} denotes the crossover elevation difference, H_i and H_j the interpolated elevations. Assuming that the interpolated elevations are biased they can be decomposed into the unbiased elevation (H_i', H_j') and the biases (a_i', a_j') themselves

$$\begin{aligned} H_i &= H_i' + a_i, \\ H_j &= H_j' + a_j. \end{aligned} \tag{2}$$

The combination of eqs (1) and (2) and a decomposition leads to

$$\Delta h_{ij} = (H_j' - H_i') + (a_j - a_i). \tag{3}$$

Richter *et al.* (2008) showed that the hydroglaciological regime of Lake Vostok is rather stable with time. The ice-surface topography above the lake is exceptionally flat and homogeneous. This reduces topography-induced interpolation errors in the crossover analysis. In addition, the snow accumulation rate is very low, on the order of 2 cm a^{-1} water equivalent (Ekaykin *et al.* 2004), and abrupt accumulation events are not common. This means, the lake area is well suited for altimeter bias determination, as it has been performed already by Shuman *et al.* (2011). If there is no significant surface-elevation change present in the area under investigation, the first term ($H_j' - H_i'$) on the right-hand side of eq. (3) vanishes and the crossover difference Δh_{ij} yields the difference of both biases a_i and a_j. This leads to the following observation equation:

$$\Delta h_{ij} = a_j - a_i + \tilde{e}, \tag{4}$$

where $\tilde{e}$ represents the sum of unmodelled elevation changes at the crossover point, including local accumulation anomalies and the response to lake tides and air pressure forcing, and the error of the altimeter measurement itself, which is considered to be an uncorrelated random variable with $E\{\tilde{e}\} = 0$ (Rummel & Sansò 1993). The RCA poses a rank deficiency, which can be solved by fixing elevation profiles as unbiased or by introducing additional constraints. The rank deficiency of the normal equation depends on the choice of the adjustment model (Schrama 1989) and equals one when one bias is estimated for each elevation profile. We introduced the constraint that the sum of all estimated biases shall be zero. The vector of the unknowns was solved by a least-squares adjustment.

We applied the RCA approach in two different ways. In a first step, we estimated one bias for each elevation profile within the area under investigation to achieve the maximum internal precision and consistency. The original elevation profiles were then corrected for these biases. This adjusted data set is referred to as solution S1. Based on these corrected elevation profiles, we generated a regional DEM of the ice-sheet surface utilizing a gridding algorithm with continuous splines in tension (Smith & Wessel 1990). This DEM has a longitude/latitude resolution of $0.^{\circ}1 \times 0.^{\circ}025$ (approx. 2.5×2.8 km) and forms the basis for our further investigations.

In a second step, we applied the RCA approach to estimate one average bias for each LOP. The result is referred to as solution S2. This set of biases can be used to derive unbiased ICESat altimetry data also in regions where the ice-surface elevation changes with time. We analysed the performance of the RCA by comparing the crossover elevation differences of both solutions with the original data set. To minimize the impact of interpolation errors induced by the surface topography, we restricted our analysis to the lake area within the grounding line published by Popov & Chernoglazov (2011).

2.2 Performance of the RCA

Fig. 3 shows the histograms of the crossover elevation differences. For the crossover elevation differences of the original, uncorrected profiles we obtained a root mean square (rms) value of 11.1 cm. The histogram in Fig. 3(a) shows a symmetric distribution about the maximum located at 4.4 cm. The application of the RCA reduced the crossover elevation differences significantly. We obtained rms values of 5.2 and 6.8 cm for S1 and S2, respectively. This corresponds to a reduction of 61 per cent (in terms of rms) for S2. The histograms for S1 (Fig. 3b) and S2 (Fig. 3c) show a much narrower distribution with the maximum at zero.

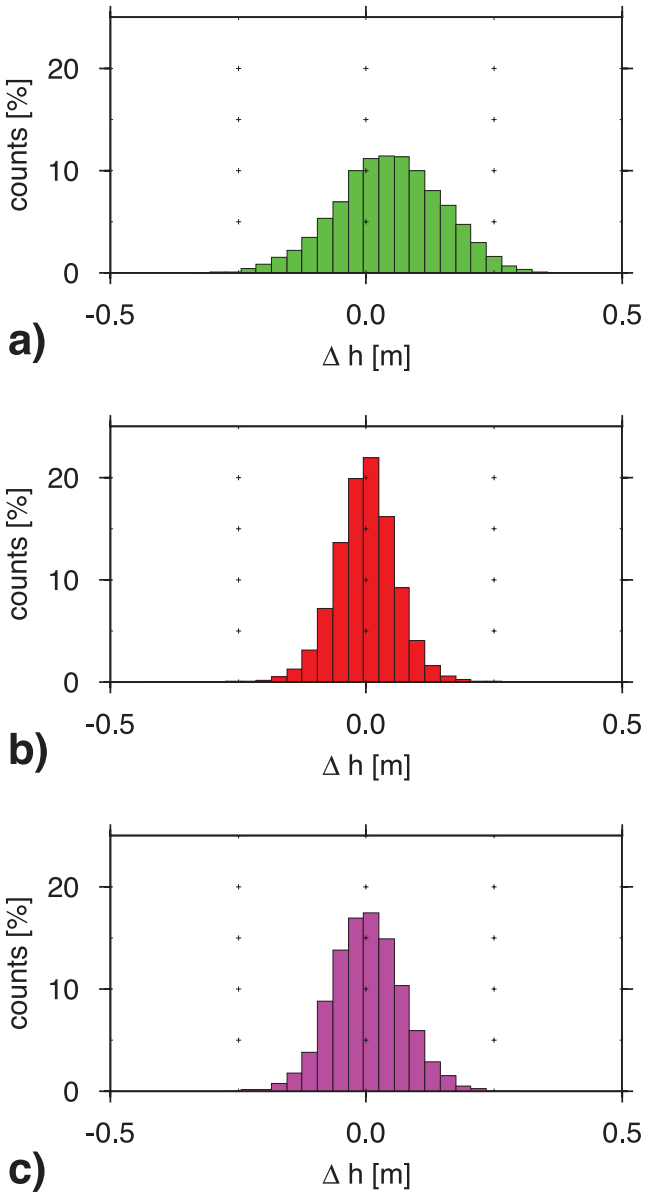

Figure 3. Histograms of the crossover elevation differences for crossovers located within the Lake Vostok area before (a) and after the regional crossover adjustment (S1) of individual offsets for each profile (b) and average biases (S2) for each LOP (c).

Table 1. ICESat average laser operational period (LOP) biases determined at Lake Vostok based on a regional crossover adjustment approach (S2).

LOP	Bias (cm)	LOP	Bias (cm)
1A	+3.9 ± 2.1	3F	−0.1 ± 1.1
2A	−0.2 ± 1.9	3G	−7.5 ± 1.2
2A	+4.3 ± 1.8	3H	−0.9 ± 1.3
2B	+3.8 ± 1.7	3I	−6.0 ± 1.4
2C	−5.1 ± 1.6	3J	−6.1 ± 1.6
3A	+13.3 ± 1.4	3K	−7.3 ± 1.8
3B	+13.9 ± 1.3	2D	−4.0 ± 1.9
3C	+4.2 ± 1.3	2E	−2.0 ± 2.0
3D	+1.8 ± 1.2	2F	−4.1 ± 2.3
3E	−1.9 ± 1.1		

Table 1 and Fig. 4(a) show the LOP biases obtained with S2. For LOP 2A, we estimate two independent biases to take into account the different repeat orbits (8- and 91-d) in which the satellite has been operated. All biases are adjusted ICESat elevations minus original ICESat elevations. They range from −7.5 (3G) to +13.9 cm (3B). The first periods up to LOP 3D are mainly positive in sign (Fig. 4) whereas the biases from LOP 3E to 2F are all negative. The largest biases were estimated for LOP 3A (+13.3 ± 1.4 cm) and 3B (+13.9±1.3 cm). The bias uncertainties (1σ) derived from a formal error propagation vary between ±1.1 and ±2.3 cm. Shuman *et al.* (2011) analysed ICESat altimetry data over subglacial Lake Vostok (see Fig. 4b) and Recovery Lakes to derive laser campaign biases. In contrast to our approach, they referenced the biases to campaign 3J. Therefore, the obtained biases are not comparable in an absolute sense, but the relative changes between successive LOP biases show a good agreement. Shuman *et al.* (2011) obtained the largest biases for campaigns 3A and 3B, too. Large biases are associated with the first LOPs of each of the three independently working lasers. Shuman *et al.* (2011) demonstrated that the estimated biases correlate strongly with the transmitted and received laser energy. The range of our LOP biases (−7.5 to +13.9 cm) corresponds to the results of Kotlyakov *et al.* (2011), who analysed ICESat altimetry data above Lake Vostok without consideration of LOP biases, interpreting them as vertical surface displacements of up to 20 cm in amplitude.

The determination of ICESat LOP biases is the subject of several publications. Important results are compiled in Siegfried *et al.* (2011). Fricker *et al.* (2005) compared ICESat elevation profiles from LOP 2A to 3C crossing the Salar de Uyuni (Bolivia) with a DEM derived from Global Positioning System (GPS) data. They determined elevation biases ranging from −33.0±4.8 cm (2C, track 085) to +102.5 ± 3.7 cm and +85.0 ± 53.4 cm (3B, tracks 085 and 360) and demonstrated that the biases are induced by environmental and instrumental effects. Gunter *et al.* (2009) derived intercampaign biases over the global ocean. They compared the ICESat elevation profiles to a mean sea-surface topography model (Urban & Schutz 2005). Their biases show a much smaller variation. LOP biases determined recently by Urban are presented by Siegfried *et al.* (2011). These biases range from −9.1 (2E) to 6.6 cm (2A). Siegfried *et al.* (2011) compared four passes (3I, 3J, 2D, 2E) of ICESat track 0412 to precise GPS surveys revealing biases between −12.1 ± 7.1 (2E) and +11.2±3.0 cm (3J). One reason for the differences in the biases could be due to the differing nature of the surface (ice, ocean, salt) in the test areas, causing differing signal backscatter characteristics. In addition, the differences in the time spans considered in the investigations may contribute to the differences in the reported biases. Moreover, the LOP biases from different publications rely on different ICESat data releases (428, 531) and thus different processing schemes, which may also slightly affect the results. Fig. 4(b) shows the sets of LOP biases determined by Shuman *et al.* (2011), Urban (Siegfried *et al.* 2011) and Siegfried *et al.* (2011).

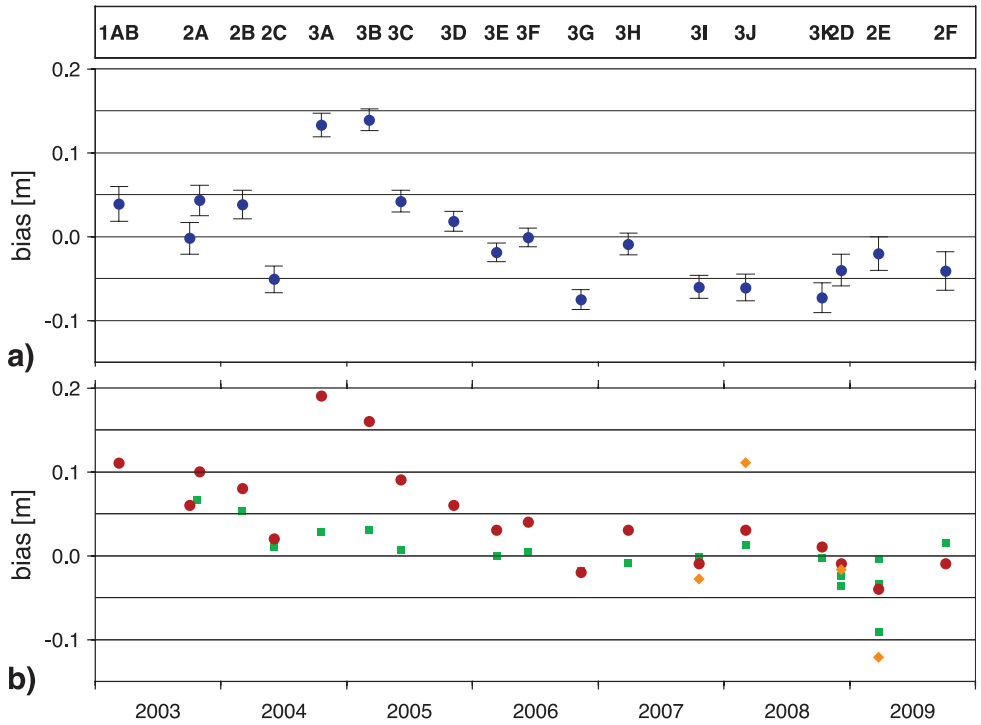

Figure 4. (a) ICESat LOP biases and their uncertainties determined over the Lake Vostok area applying a regional crossover adjustment approach (S2). (b) ICESat LOP biases from different authors for comparison. Red dots: Shuman *et al.* (2011), green squares: Urban (Siegfried *et al.* 2011) and orange diamonds: Siegfried *et al.* (2011) (LOP 3I, 3J, 2D, 2E). All biases are corrected elevation minus original ICESat elevation.

The LOP biases as stated in different publications vary in magnitude and sometimes even in sign. This needs further analysis, especially in the view of Antarctic and Greenlandic mass-balance determinations based on time-series of ICESat elevation profiles. The LOP biases dominate the mass balance estimates in regions of low accumulation and ablation (e.g. East Antarctica). Hence, a reliable estimation of the Antarctic and Greenlandic mass balance requires the introduction of correct ICESat LOP biases.

Furthermore, we compared our individual elevation biases (S1) to the corresponding LOP biases (S2). The S1 biases show a larger variation within each LOP than expected on the basis of the formal uncertainties of the average LOP biases themselves. Therefore we conclude, that there is a significant short-term variation of the biases within each LOP which cannot be neglected for high-accuracy applications.

2.3 Validation of the ice-surface DEM

The DEM derived from our adjusted data set S1 (provided in the Supporting Information section online) is plotted in Fig. 5(a). It shows that the ice sheet over the lake is characterized by a very smooth surface. The signal content of the ice-surface topography for wavelengths ranging from 1 to 10 km is close to zero. Between the northern and the southern parts of the lake, over a distance of about 240 km, the surface elevation changes by just 50 m. Outside the lake area, the ice surface has much more signal content on shorter wavelengths (visible also in the SAR-mosaic in Fig. 1). For the validation and accuracy assessment of our ice-surface DEM, we utilized three independent data sources.

First, the internal precision of the DEM was evaluated based on the adjusted S1 data set itself. The largest uncertainties are expected within the meshes between the ascending and descending elevation profiles. Different test DEMs were generated excluding individual repeat tracks. These DEMs were interpolated to the locations of the footprints of the tracks excluded from the DEM generation. The interpolated elevations were then compared with the adjusted altimetry measurements. This was done for four repeat tracks (71, 92, 443 and 1178; see Fig. 2).

Table 2. rms of the elevation differences derived from the original profiles and the profiles interpolated from the corresponding ice surface DEMs. The rms values were calculated for the whole area under investigation and the lake area only. The last row denotes the over all rms including all four profiles.

Track #	Lake—rms (m)	Whole area—rms (m)
71	0.48	1.55
92	0.67	2.98
443	0.62	1.75
1178	0.76	1.99
over all	0.61	2.14

Table 2 shows the rms values of the obtained elevation differences distinguishing between the lake area and the overall region under investigation. In the lake area, track 71 yields the smallest rms of 0.48 m. This track crosses the lake close to its centre line in north–south direction. The largest rms (0.76 m) was obtained for track 1178, which crosses the southern part of the lake from west to east. Taking all four tracks into account, the rms of the elevation differences over the lake and the entire region amount to 0.61 and 2.14 m, respectively. It should be noted, that our test points along the omitted repeat tracks are separated from the next included profile by a distance corresponding to the typical mesh width (approximately 15 km; Fig. 2). On average, an arbitrary point is less distant from the closest profile, thus the obtained rms values represent

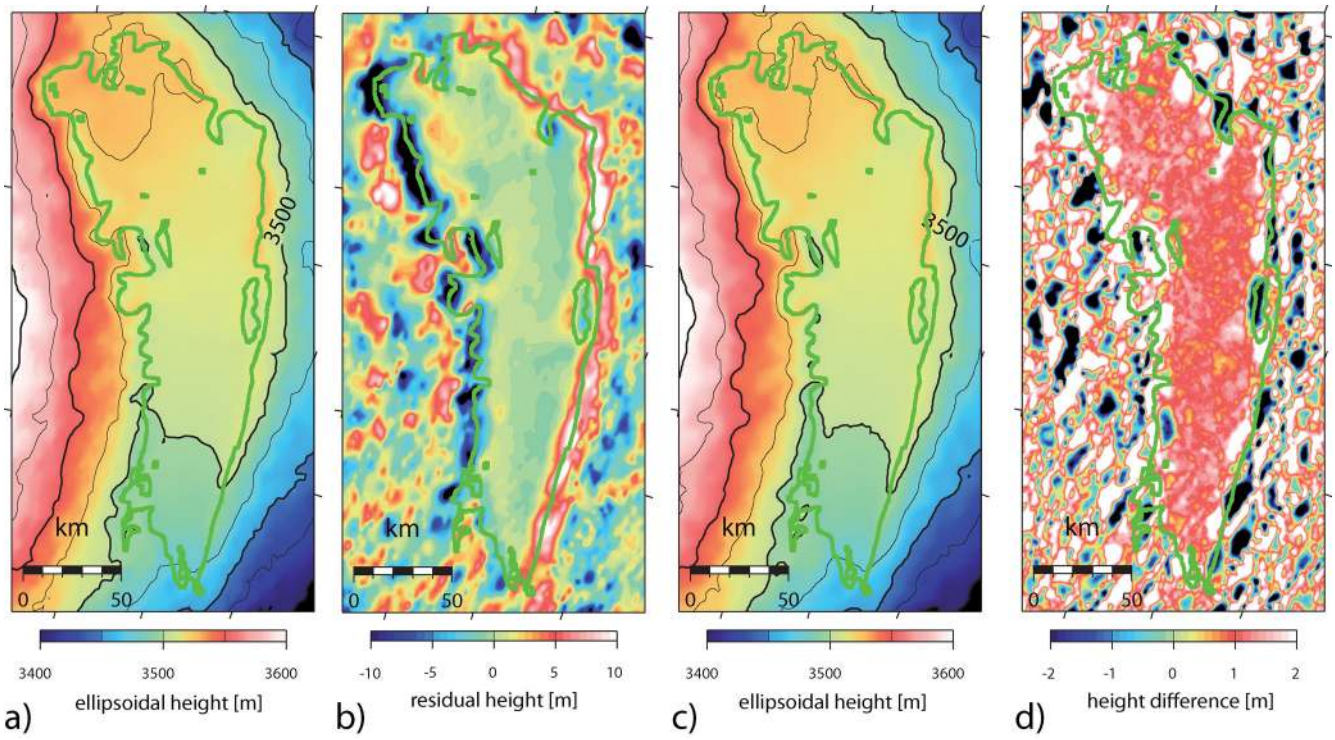

Figure 5. (a) ICESat-derived DEM of the ice surface. (b) Residual DEM after the application of a high-pass filter. (c) DEM of the ice surface derived from ERS-1 radar altimetry data (Roemer *et al.* 2007). (d) Difference of the ICESat-DEM (a) minus the ERS-1 DEM (c). Ellipsoidal heights are given with respect to the TOPEX reference ellipsoid.

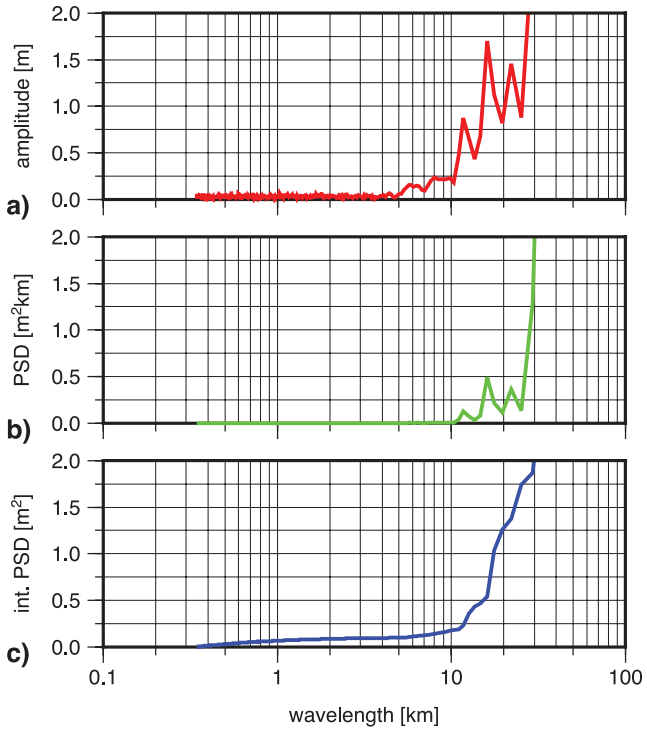

Figure 6. Spectra of the surface elevation variations along ICESat track 443. (a) amplitude spectrum; (b) power spectral density (PSD) and (c) integrated PSD as a function of the wavelength.

an upper limit for the uncertainty of our DEM. We conclude that the uncertainty does not exceed 0.76 m over Lake Vostok. Outside the lake, the uncertainties are larger due to the increased variance of the topography on shorter wavelengths. The uncertainty of the DEM over the entire region under investigation is estimated to be 2.1 m.

A spectral analysis was performed for one elevation profile of reference track 443. The amplitude spectrum of this profile is depicted in Fig. 6(a). It indicates amplitudes close to zero for wavelengths shorter than 5 km. Fig. 6(b) shows the power spectral density (PSD) and Fig. 6(c) the integrated signal power as a function of the wavelength. For wavelengths up to 10 km, the integrated power amounts to 0.2 m^2. This corresponds to only 0.05 per cent of the total power. The integrated power for the average mesh width of 15 km amounts to 0.45 m^2, only slightly larger than the variance (0.38 m^2) corresponding to the rms of the differences between interpolated and measured elevations over the lake (0.62 m; Table 2) and thus confirming our accuracy assessment.

In a second approach, we compared our DEM with the ice-surface DEM (see Fig. 5c) published by Roemer *et al.* (2007). That model is based on ERS-1 radar altimetry (RA) data. Roemer *et al.* (2007) applied a refined data analysis method to minimize the slope induced-error which is the most important limitation of RA missions. The radar-derived DEM, initially given with respect to the GRS80 reference ellipsoid, was converted to the TOPEX/Poseidon reference ellipsoid to which our DEM refers.

Fig. 5(d) shows the DEM differences between ICESat and ERS-1. The lake and its shoreline is clearly perceivable. Over the lake, the differences are very homogeneous with the RA-derived DEM being, on average, 1.19 m lower than our laser-based DEM. This is mainly caused by the differences in the signal characteristics. RA operates with signal pulses at 13.8 GHz (Ku-band) and maps the ice-sheet surface at a lower level than the laser altimetry due to the effect of volume-scattering of the radar signal. In contrast to that, the ICESat laser signal is reflected at the atmosphere-firn interface directly (surface reflection). According to Davis & Zwally (1993), the penetration depth of the RA signal in Antarctica ranges from 5 to 10 m. Davis (1997) showed that in flat terrains the altimeter height may be underestimated by 0.5–1.5 m (10 per cent threshold in the altimeter-retracking algorithm) or even 1–3 m (50 per cent threshold). Roemer *et al.* (2007) compared their RA-derived DEM with airborne laser-altimeter measurements (Studinger *et al.* 2003) and obtained an offset of 1.6 ± 0.6 m, in good agreement with our result. Considering the almost constant elevation difference within the lake area, we see no indication of inhomogeneous firn conditions. Outside the lake, the elevation differences show undulations of positive and negative sign matching the pattern of the ICESat reference tracks. The largest elevation differences are found within the meshes of the ICESat tracks. There they vary between -5.0 and $+5.0$ m. Along the tracks, they are within -1.0 and $+2.0$ m. The increased variance of the elevation differences outside the lake area is due to the increased roughness of the surface topography. In the generation of the ICESat-derived DEM, these topographic features increase the uncertainties of the elevations resulting from interpolation between the ICESat elevation profiles (i.e. within the meshes). The ERS-1-derived DEM is affected by the same effect. In addition, the topographic roughness outside the lake increases the slope-induced elevation error, which is the most limiting factor of the RA. Applying a constant offset of $+1.19$ m to the RA-derived DEM the rms of the elevation difference with respect to our ICESat-derived DEM over the lake amounts to 0.40 m. This value includes the uncertainties of both ice-surface DEMs.

Thirdly, we used surface elevations determined by GPS as independent data source for a comparison with our DEM. These elevations were obtained for 34 GPS markers well distributed over the northern and southern parts of the lake (Fig. 2). Vostok station was excluded from this analysis because its buildings cause accumulation anomalies which affect the local ice-surface elevation. However, such small-scale surface features are below the spatial resolution of the GLAS data. The markers were observed by GPS during the Antarctic field seasons between 2001 and 2008 with observation times ranging from several hours to 10 days (Wendt *et al.* 2006; Richter *et al.* 2008). The GPS data were processed using the Bernese GPS software 5.0 (Dach *et al.* 2007) yielding 3-D site coordinates. The obtained coordinates were transformed from the WGS84 to the TOPEX reference ellipsoid. The heights derived from GPS were converted from the tide-free system, in which they are originally given, to the mean-tide system, which is used in altimetry, by adding the geometrical effect of the permanent tide of -23.7 cm.

In a first step, we examined four GPS sites which are located close to the centre of ICESat footprints within distances between 22 and 80 m (Fig. 2). At these sites, the obtained elevation differences range from $+17.8$ to $+29.2$ cm with a mean value of $+21.7 \pm 5.2$ cm. Even without accounting for slope-induced elevation differences between the GPS sites and footprint centres, the bias (21.7 ± 5.2 cm) is only slightly larger than the expected absolute single shot accuracy of ICESat of about ± 15 cm (Zwally *et al.* 2002). However, the number of observation sites is not regarded as being sufficient enough to constrain the adjusted ICESat elevation profiles to the absolute elevation reference of the GPS elevations.

Therefore, in a second step, we compared the DEM with the complete GPS data set. For this purpose, the DEM was interpolated to

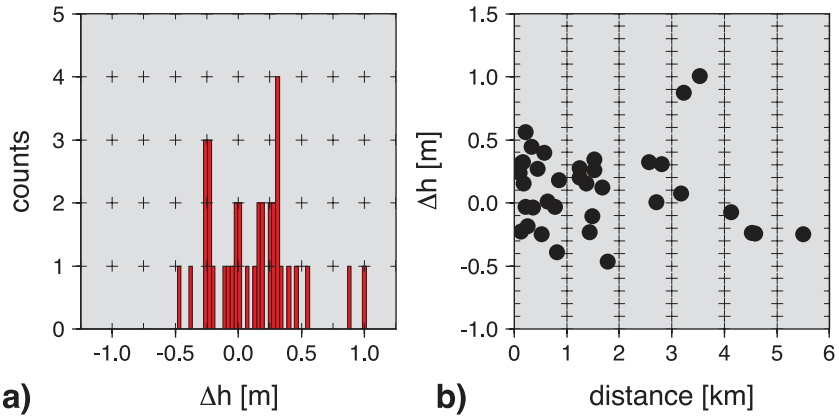

Figure 7. (a) Histogram of the obtained elevation differences from the comparison of the ICESat-derived ice surface DEM and the GPS data. (b) Elevation differences as a function of the distance to the closest ICESat elevation profile.

the GPS sites. Fig. 7(a) shows the histogram of the differences between the DEM and GPS elevation. The elevation differences range from −46.7 to +100.6 cm with a mean value of +11.3 ± 32.4 cm. Fig. 7(b) depicts the elevation differences as a function of the distance to the closest ICESat elevation profile included in the DEM generation. For 27 GPS sites (79 per cent), the distance to the closest ICESat elevation profile is below 3 km. The maximum difference (+100.6 cm) was found for a distance of 3.5 km. However, also within 1 km the elevation differences reach −39.1 and +55.9 cm, respectively, and there is no clear correlation between the elevation difference and the distance. Therefore, we used the overall mean of +11.3 cm, based on the complete set of GPS sites regardless of their distances, to tie the adjusted ICESat elevation data to the GPS elevation reference. The standard deviation of ±32.4 cm reflects the impact of various sources of uncertainty. Although the GPS elevations are point measurements, ICESat provides the average elevation of the entire illuminated footprint. The impacts of both microtopography (sastrugi) and interpolation effects of the gridding algorithm in the DEM generation are difficult to quantify. Neglecting both and assuming an accuracy of ±2 cm for the GPS measurements, a formal error propagation leads to an accuracy of the DEM of ±32 cm close to the ICESat profiles. From this, an absolute single shot accuracy of the GLAS measurement of 30 cm or better can be inferred. This estimate is in agreement with results of Magruder *et al.* (2007) who compared level-1B (GLA06) elevation data with an airborne lidar survey of the White Sands Space Harbor in New Mexico. Their comparison showed an agreement of ±34 cm in general and ±6.7 cm under best conditions. Our results confirm that the absolute accuracy of the ICESat-derived DEM is significantly better than ±0.7 m (as determined above as upper limit) within a distance of few kilometres from the elevation profiles.

The ICESat-derived ice-surface DEM provides insights into the properties of the ice sheet above Lake Vostok. For this purpose, the DEM was high-pass filtered with a cut-off wavelength of 50 km. The filtered DEM is displayed in Fig. 5(b). It shows peculiar topographic features of the ice surface, which extend along the shorelines of the lake. A depression with an average depth around 10 m is observed at the western shoreline, whereas a bump is found at the eastern shoreline. Along the shoreline, their width varies between 10 and 15 km. These ice-surface features at Lake Vostok were already reported by Rémy *et al.* (1999), although they stated a slightly smaller magnitude of the elevation anomaly (6 m) and an average width of 10 km. The topographic features are orientated perpendicular to the main ice flow direction from west to east (Wendt *et al.* 2006) and represent surface manifestations of local changes of the ice flow regime at the grounding line. At the northern and southern shorelines, which are aligned with the general ice flow direction, these features are absent.

3 THE HYDROSTATIC EQUILIBRIUM AT LAKE VOSTOK

3.1 Data

In addition to an ice-surface DEM, two other types of data are needed for a quantitative evaluation of the HE of floating ice: an ice-thickness model and a geoid model.

The ice-thickness model used in this work results from the combination of two different RES data sets. The first set comprises a total of 5190 km of ground-based RES profiles collected by the Polar Marine Geosurvey Expedition in the framework of the Russian Antarctic Expedition between 1998 and 2008 (Masolov *et al.* 2006; Popov & Masolov 2007). The second set was obtained during the US airborne geophysical survey campaign 2000/2001 (Studinger *et al.* 2003) and consists of a regular grid merging 12 464 km of RES profiles covering the Lake Vostok region. Both sets of RES data were reprocessed and the resulting ice-thickness data were merged into the combined model depicted in Fig. 8(a) (Siegert *et al.* 2011). An individual crossover analysis for both data sets revealed a comparable standard deviation of 42 and 39 m for the Russian and US data, respectively. For the merged set of profiles, a standard deviation of 65 m was obtained at 1717 crossovers. A significant contribution to this standard deviation is due to a small number (less than 5 per cent) of crossovers which exhibit differences exceeding 150 m and which are situated almost exclusively in locations of very rough bedrock relief.

A regional geoid model (Fig. 8b) was derived from free-air gravity anomaly data acquired during the 2000/2001 airborne geophysical survey (Studinger *et al.* 2003). In the computation, the remove–compute–restore technique with collocation was applied (Forsberg & Tscherning 1981). The GOCE global gravity field model in release 2 (GO_CONS_GCF_2_TIM_R2) based on the timewise approach and available up to degree/order 250 (Pail *et al.* 2011) was introduced representing the long-wavelength part. A residual terrain model resulting from a high-pass filtered consistent model of ice-surface elevation was used to represent the short-wavelength part. A detailed description of the applied approach for

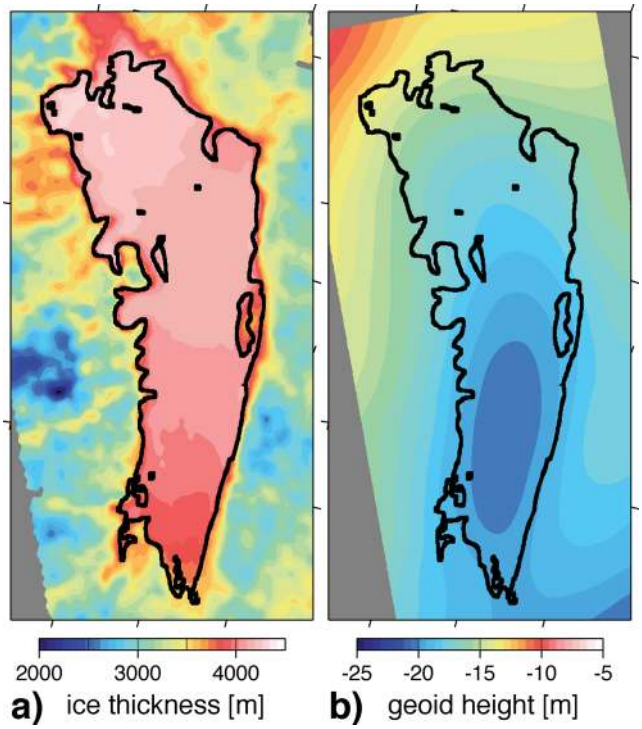

Figure 8. (a) Ice-thickness model covering the Lake Vostok area based on RES data (Siegert *et al.* 2011). (b) Regional improved geoid model introduced in the evaluation of the hydrostatic equilibrium.

regional geoid determination in Antarctica can be found in Scheinert *et al.* (2008).

3.2 Methodology

An ice floe freely floating in open water is in HE. The extent to which the ice sheet above Lake Vostok fulfils the HE condition was evaluated based on our ICESat-derived DEM and the ice-thickness and geoid models. The hydrostatic balance relation of free-floating ice bodies is given by

$$\rho_w(Z - h) = \bar{\rho} Z \tag{5}$$

where Z is the total ice thickness, ρ_w is the mean density of the displaced water column, $\bar{\rho}$ the mean density of the ice body and h represents the elevation of the ice surface above an equilibrium level. If the extension of the water surface is larger than that of the ice floe, for example an iceberg in the ocean, this equilibrium level would be represented by the equipotential surface at the elevation of the water surface, that is, the sea level, and h would be the free board elevation. In the case of subglacial lakes, where the extension of the ice sheet exceeds that of the aquifer, the equilibrium level is also situated within the ice body, but the elevation h is not directly observable. In analogy to the iceberg/ocean example we will henceforth refer to the equilibrium level as 'apparent lake level'. It represents the fictive lake surface, if the ice in each vertical column would be melted. Eq. (5) implies that both densities are *a priori* given. For the vertically stratified ice sheet, the mean density $\bar{\rho}$ depends on the total ice thickness as well as on the accumulation and densification regime in the upper firn layers. According to Fig. 8(a), the ice thickness above Lake Vostok ranges from 3750 to 4150 m. This implies slight changes of $\bar{\rho}$ even for a homogeneous accumulation and densification regime (Section 2.3). According to Horwath *et al.* (2006), this can be dealt with by reformulating eq. (5) in the following way:

$$\rho_w(Z - h) = \rho_i(Z - \delta), \tag{6}$$

where δ is the deviation of the ice bodies mean density $\bar{\rho}$, vertically integrated along the column of ice, from pure ice (ρ_i). This means that the ice body is decomposed into a body of pure ice and an apparent layer of air. Furthermore, the free board elevation h is replaced by the difference of the ice-surface elevation H_I and the elevation of the apparent lake level H_S

$$h = H_I - H_S. \tag{7}$$

In the following, we assume that the apparent lake level is an equipotential surface. This specific equipotential surface can be expressed as the sum of the geoid undulation N and an offset a

$$H_S = N + a. \tag{8}$$

Strictly speaking, a varies in space. Test computations showed, however, that the variation of a within the lake area keeps below 5 cm. In the following, we regard a as a constant offset within the lake area. Substitution of eqs (7) and (8) into eq. (6) leads to

$$H_I - Z\left(1 - \frac{\rho_i}{\rho_w}\right) - N = \frac{\rho_i}{\rho_w}\delta + a. \tag{9}$$

The sum on the right-hand side can be simplified to a constant parameter b. This yields the final relation

$$H_I - Z\left(1 - \frac{\rho_i}{\rho_w}\right) - N = b. \tag{10}$$

The difference on the left-hand side represents the observation vector. The parameter b on the right-hand side denotes a constant offset which has to be determined beforehand. The assessment of the HE was thus done in two steps. In the first step, the offset b was determined by a least-squares adjustment for a central section (E) of the lake, for which the HE condition was assumed to be fulfilled. The contour of this test section was chosen based on a SAR-mosaic (Jezek & RAMP product team 2002, see Fig. 1) and the lake shoreline inferred from RES data (Popov *et al.* 2006; Popov & Chernoglazov 2011). It is included in Fig. 10(d). Subsequently, the HE was evaluated for all DEM grid nodes within the lake area applying the obtained b value in eq. (10). The application of eq. (10) for the evaluation of the fulfilment of the HE is referred to in the following as approach A1. The geometrical meaning of the involved quantities is illustrated in Fig. 9.

In eq. (10), two density assumptions were introduced. Based on findings for pure ice bodies published by Horwath *et al.* (2006), we used a density value of 917.0 kg m^{-3}. Previous investigations based on lake water circulation models and the HE condition suggest that the water of Lake Vostok may be slightly salty (Siegert *et al.* 2001; Kapitsa *et al.* 1996). In our analysis, we applied a water density of 1016.0 kg m^{-3} according to Wüest & Carmack (2000).

In addition, eq. (10) can be rearranged as follows:

$$H_I - N = Z\left(1 - \frac{\rho_i}{\rho_w}\right) + b. \tag{11}$$

Here, both the offset b and the factor $(1 - \frac{\rho_i}{\rho_w})$ have to be determined in the first step. This second approach A2 allows the lake water density to be estimated using the assumed density of pure ice ρ_i. A formal least-squares adjustment is not applicable in this case because the ice-thickness values contained in the design matrix are subject to uncertainties, too. Therefore, an iterative approach was used to fit a linear regression model to the data set.

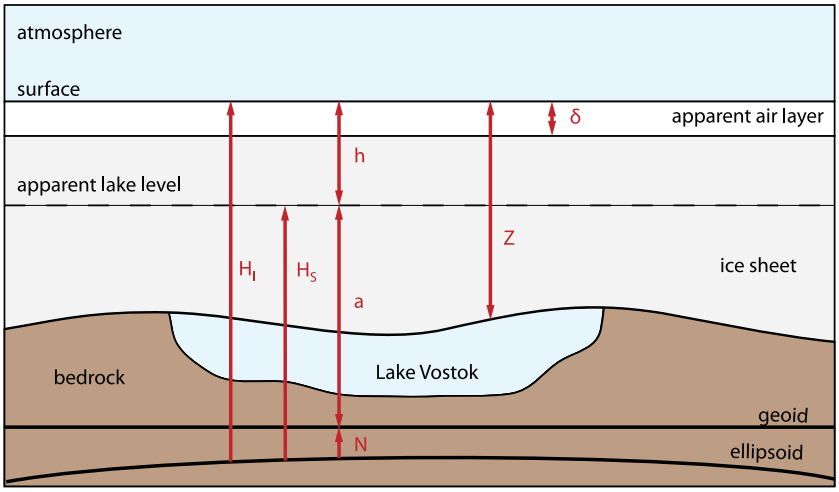

Figure 9. Geometrical relationships between the components which are needed for the investigation of the hydrostatic equilibrium at Lake Vostok.

After the determination of the elevation of the apparent lake level, the local metric deviation *HE* of the ice surface from the HE condition is estimated according to

$$HE = H_I - Z\left(1 - \frac{\rho_i}{\rho_w}\right) - N - b. \quad (12)$$

The HE is fulfilled when the right-hand side equals zero. In the following, we apply eq. (12) to our Lake Vostok data sets.

3.3 Results and discussion

Both approaches A1 and A2 were applied to determine the constant parameter *b*. Furthermore, to assess the uncertainty of the determined offset independently from the formal error propagation in the least-squares adjustment, the test section (E) was divided into the three subsections shown in Fig. 10(d): north (N), centre (C) and south (S). The offset determination was repeated for each subsection. The obtained results with their formal uncertainties are compiled in Table 3. The application of approach A1 to the entire test section (E) yields an offset of 3129.688 ± 0.006 m. For the same area, an offset of 3137.708 ± 0.396 m is obtained by approach A2, which is 8 m larger than the result of A1. The variation range of the offsets obtained for the three subsections (north, centre, south) applying approach A1 (0.5 m) is significantly smaller than that resulting from A2 (19 m). Approach A2 yields, in addition to the offset, also the density ratio between ice and lake water. The ratio obtained for the entire test section (E) corresponds to a density of the lake water of 1013.81 kg m^{-3} when assuming an ice density of 917.0 kg m^{-3}. This water density is 2.2 kg m^{-3} lower than that suggested by Wüest & Carmack (2000). The water

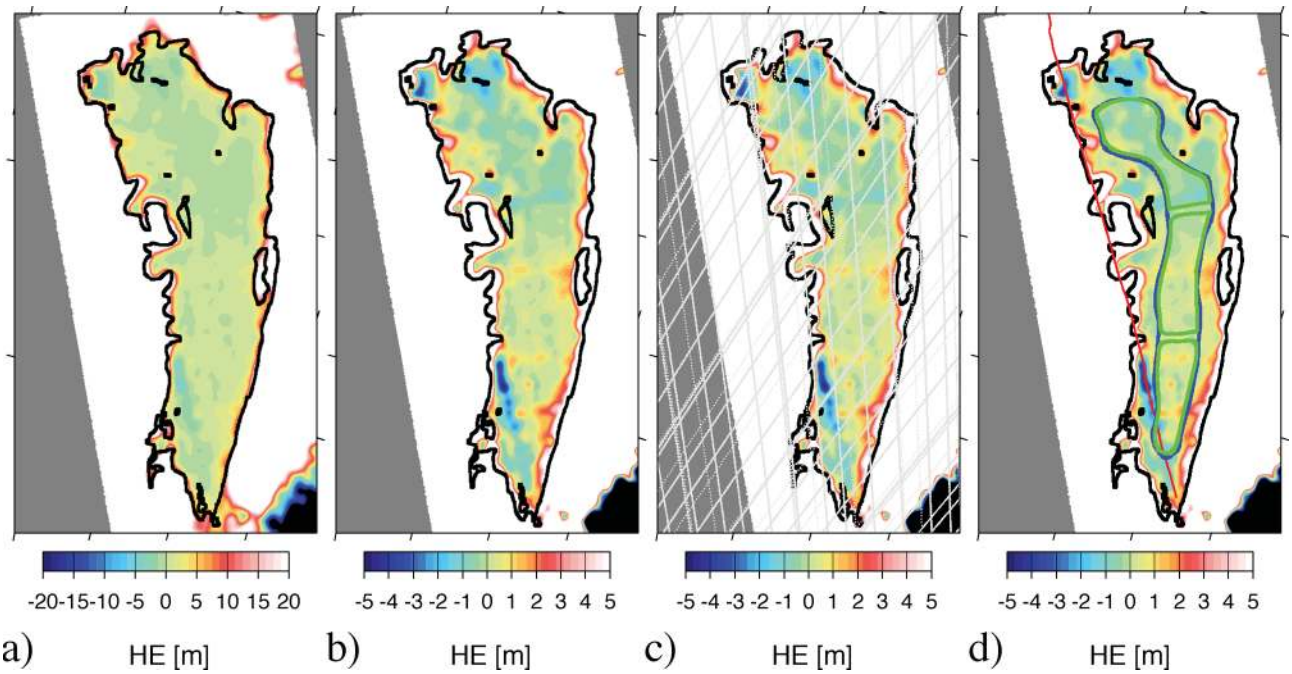

Figure 10. Deviation from the hydrostatic equilibrium colour coded within a bound of ±20 m (a) and ±5 m (b). (c) Deviation from the hydrostatic equilibrium in combination with the locations of the ICESat elevation profiles. (d) HE deviation. The convoy route Vostok–Mirny is depicted in red. The lake areas which have been used for the offsets determination (first step) are shown in blue and green.

Table 3. Compilation of the offsets b in the HE equation determined by both applied approaches (A1, A2) for the four test areas E, N, C and S. For A2, the estimated lake water density is included, assuming an ice density of 917 kg m^{-3}.

Area	A1	A2	
	offset (m)	offset (m)	ρ_w (kg m^{-3})
E	3129.688 ± 0.006	3137.708 ± 0.396	1013.81 ± 0.05
N	3129.391 ± 0.008	3123.843 ± 0.844	1017.49 ± 0.21
C	3129.844 ± 0.005	3140.519 ± 0.928	1013.11 ± 0.24
S	3129.895 ± 0.014	3121.375 ± 1.387	1018.40 ± 0.35

densities obtained for the three subsections vary between 1013.11 (C) and 1018.40 kg m^{-3} (S). The differences between the offsets and densities obtained for the three subsections all exceed their formal errors and thus suggest that the applied least-squares adjustment (A1) and linear regression (A2) both underestimate the real uncertainties. Although spatial lake water density variations are conceivable due to basal melt and accretion processes (Siegert *et al.* 2001), it is more likely that the obtained density variation between the subsections is a result of the applied approach. The regression model is highly sensitive to the density ratio. However, a slight change in the density assumptions in approach A1 results in a change of offset b but has little effect on the HE determination. We therefore applied the bias resulting from approach A1 for the entire test section (E) in the HE assessment.

In the formal error propagation of the obtained HE values, four sources of uncertainty are considered. The largest uncertainty contribution results from the ice-thickness data. Crossover analysis of the independent ice-thickness data sets revealed a formal uncertainty of about 65 m (see Section 3.1). That uncertainty should be an upper limit appropriate for the ice-thickness model outside the lake area. Richter *et al.* (2008) estimated an ice-thickness uncertainty of about ±11 m close to Vostok station. This result is confirmed by the findings of Popov *et al.* (2003) (±15 m). In the following, we assume an ice-thickness uncertainty of 15 m for the lake area. This error translates into a HE uncertainty of about 1.4 m. The second largest contribution is due to the uncertainties of the ice-surface DEM derived from ICESat (better than 0.7 m). Furthermore, the regional geoid model is estimated to contribute 0.05 m to the HE uncertainty. The formal uncertainty of offset b amounts to 0.006 m (approach A1, entire lake section). This value does not account for spatial variations of the offset a (Section 3.2). The total uncertainty contribution of parameter b is therefore estimated to be 0.05 m. The density ratio between the values assumed for ice and lake water is assumed to be constant over the lake area and is considered as error-free. A change in the density ratio would just result in a slight change in b in the first step of the HE determination. The formal uncertainty of the HE values is thus ±1.6 m.

Figs 10(a) and (b) show the deviation from the HE for Lake Vostok. Over large parts of the lake, the HE keeps within a range of ±1 m. This applies also outside the test section used for the offset determination. Along the lake shoreline, there is a positive deviation from the HE of up to +10 m, which reproduces well the general outline of the lake (Fig. 10a). This anomaly indicates parts of the ice sheet which are either grounded on bedrock outside the lake or in the transition zone between grounded and freely floating ice. Small bays as well as the narrow passage between a large bedrock island and the eastern shoreline do not manifest themselves in the HE plot. Their areal extent is too small compared to the width of the transition zone. The latter is expected to be two to three times the ice thickness, that is about 10 km at Lake Vostok (Vaughan 1994; Rémy *et al.* 1999). From our HE assessment, we inferred a width of the transition zone of 10–15 km. Especially in the southern part of the lake, this zone appears to be wider.

Fig. 10(b) shows slightly positive HE deviations in the southern part of the lake whereas in the northern part slightly negative deviations are obtained. In the northern part of the lake, the fresh water input due to basal melting might decrease the density of the slightly saline water, whereas accretion processes in the southern part would increase the water density (Thoma *et al.* 2008). Localized geothermal heating at the bottom of the lake might also produce spatial variations in the water density (Siegert *et al.* 2001). In the approaches applied for the HE assessment, differences in the lake water density would manifest themselves in differences in the HE values.

RES data (Popov *et al.* 2006; Popov & Chernoglazov 2011) revealed a number of sites in the northern part of the lake where the ice sheet is grounded upon small islands (Fig. 10b). At two islands close to the centre of the northern part our analysis yields, as expected, positive deviations of +3 m. In contrast, two islands close to the northern shore exhibit a negative HE deviation (−1.5 m; Fig. 10b) instead of a positive deviation. Furthermore, the elongated island detected by RES close to the western shore (77.2°S) does not exhibit a distinct positive HE deviation (±1 m). A closer look at the location of the ICESat profiles in Fig. 10(c) shows that they just touch the perimeter of the elongated island and that most of the small islands fall within the profile meshes. Thus, surface manifestations of grounded ice may not always be represented in the ICESat-derived DEM when they are too small and/or unfavourably located with respect to the profiles.

Fig. 10(b) indicates a strong negative deviation (up to −4.0 m) in the southern part of the lake close to the western shore. This anomaly coincides with the convoy track Vostok–Mirny included in Fig. 10(d). For about 50 yr, this track has been used twice a year by the heavy vehicles of the logistic convoy of the Russian Antarctic Expedition to supply Vostok station. The load of the vehicles enhanced the densification of the upper firn layers leading to a local increase of the mean ice density (or a thinner apparent air layer) along the track. In the HE assessment, where homogeneous accumulation and densification are assumed, this density anomaly translates into a negative deviation from the HE.

4 CONCLUSION

The presented analysis of the complete set of ICESat laser altimetry data over subglacial Lake Vostok provided new results for further applications of ICESat data to investigate other ice-covered regions as well as for the understanding of the interactions between subglacial lakes and the Antarctic ice sheet. We took advantage of the peculiarities of Lake Vostok: an extended, flat ice surface in HE and with negligible surface elevation change over time. We used this unique, almost ideal test area to determine ICESat LOP altimeter biases. These biases can be considered to be applied in other ice-covered regions to reduce the systematic effect of these laser biases from real temporal ice-surface elevation changes. Furthermore, the ICESat data were used to generate a regional ice-surface DEM for Lake Vostok. This DEM is free of the effects of volume reflection inherent to RA and has an accuracy of better than 0.7 m over the lake.

We applied this DEM to evaluate quantitatively to which extent the ice sheet above Lake Vostok is in HE. Our results demonstrate that the HE condition is fulfilled over almost the entire lake area

and identify the areas where the HE is violated. They show that it is essential to introduce a precise regional geoid model, as the range of the geoid height in the lake area (∼10 m) is one order of magnitude larger than the HE values over most of the lake. Our HE analysis allowed to map the generalized shoreline of the subglacial lake and, under favourable conditions, to localize islands where the ice is grounded. Very localized disturbances of the firn structure along the convoy track Vostok–Mirny are clearly reflected as HE anomalies. Our analysis provides new, independent estimates for the width of the transition zone and for the water density of Lake Vostok.

ACKNOWLEDGMENTS

We thank NSIDC for providing the GLAS data. Furthermore, parts of this work were supported by the Russian Fund for Basic Research (RFBR, grant 10-05-91330-NNIO-0430) and the German Research Foundation (DFG, grants DI-473/38 and DI-473/34-1). Additionally, we thank the editor Bert Vermeersen and the two anonymous reviewers for their constructive comments which improved the presentation of our results considerably.

REFERENCES

Abshire, J., Sun, X., Riris, H., Sirota, J., MCGarry, J., Palm, S., Yi, D. & Liiva, P., 2005. Geoscience Laser Altimeter System (GLAS) on the ICESat Mission: on-orbit measurement performance, *Geophys. Res. Lett.,* **32,** L21S02, doi:10.1029/2005GL024028.

Bell, R., Studinger, M., Tikku, A., Clarke, G., Gutner, M. & Meertens, C., 2002. Origin and fate of Lake Vostok water frozen to the base of the East Antarctic ice sheet, *Nature,* **416,** 307–310.

Dach, R., Hugentobler, U., Fridez, P. & Meindl, M.A., 2007. *Bernese GPS Software Version 5.0,* Astronomical Institute, University of Bern, Switzerland.

Davis, C., 1997. A robust threshold retracking algorithm for measuring ice-sheet surface elevation change from satellite radar altimeters, *IEEE Trans. Geosci. Remote Sens.,* **35**(4), 974–979.

Davis, C. & Zwally, H., 1993. Geographic and seasonal variations in the surface properties of the ice sheets by satellite-radar altimetry, *J. Glaciol.,* **39,** 687–697.

Ekaykin, A., Lipenkov, V., Kuzmina, I., Petit, J., Masson-Delmotte, V. & Johnsen, S., 2004. The changes in isotope composition and accumulation of snow at Vostok station, East Antarctica, over the past 200 years, *Ann. Glaciol.,* **39,** 569–575.

Forsberg, R. & Tscherning, C., 1981. The use of height data in gravity field approximation by collocation, *J. geophys. Res.,* **86**(B9), 7843–7854.

Fricker, H., Bassis, J., Minster, B. & MacAyeal, D., 2005. ICESat's new perspective on ice shelf rifts: the vertical dimension, *Geophys. Res. Lett.,* **32,** L23S08, doi:10.1029/2005GL025070.

Gunter, B. *et al.*, 2009. A comparison of coincident GRACE and ICESat data over Antarctica, *J. Geod.,* **83**(11), 1051–1060.

Gysen, H.V. & Coleman, R., 1997. On the satellite altimeter crossover problem, *J. Geod.,* **71,** 83–96.

Horwath, M., Dietrich, R., Bäßler, M., Nixdorf, U., Steinhage, D., Fritzsche, D., Damm, V. & Reitmayr, G., 2006. Nivlisen, an Antarctic ice shelf in Dronning Maud Land: geodetic-glaciological results from a combined analysis of ice thickness, ice surface height and ice flow observations, *J. Glaciol.,* **52**(176), 17–30.

Jezek, K. & RAMP product team, 2002. *RAMP AMM-1 SAR Image Mosaic of Antarctica,* Alaska Satellite Facility, Fairbanks, AK, in association with the National Snow and Ice Data Center, Boulder, CO.

Kapitsa, A., Ridley, J., Robin, G. de Q., Siegert, M. & Zotikov, I., 1996. A large deep freshwater lake beneath the ice of central East Antarctica, *Nature,* **381,** 684–686.

Karl, D., Bird, D., Björkman, K., Houlihan, T., Shackelford, R. & Tupas, L., 1999. Microorganisms in the accreted ice of Lake Vostok, Antarctica, *Science,* **286,** 2144–2147.

Kotlyakov, V., Vasiliev, L., Kachalin, A., Moskalevskii, M. & Tyuflin, A., 2011. Punctuated equilibrium of the surface above subglacial Lake Vostok in Antarctica, *Doklady Earth Sci.,* **438**(1), 649–651.

Luthcke, S., Rowlands, D., Williams, T. & Sirota, M., 2005. Reduction of ICESat systematic geolocation errors and the impact on ice sheet elevation change detection, *Geophys. Res. Lett.,* **32,** L21S05, doi:10.1029/2005GL023689.

Magruder, L., Webb, C., Urban, T., Silverberg, E. & Schutz, B., 2007. ICESat altimetry data product verification at White Sands Space Harbor, *IEEE Geosci. Remote Sens. Lett.,* **45**(1), 147–155.

Masolov, V., Popov, S., Lukin, V., Sheremetyev, A. & Popkov, A., 2006. Russian geophysical studies of Lake Vostok, Central East Antarctica, in *Antarctica: Contributions to Global Earth Sciences,* pp. 135–140, Springer, New York, NY.

Nguyen, A. & Herring, T., 2005. Analysis of ICESat data using Kalman filter and kriging to study height changes in East Antarctica, *Geophys. Res. Lett.,* **32,** L23S03, doi:10.1029/2005GL024272.

NSIDC, 2011. *GLAS Altimetry Product Usage Guidance,* National Snow and Ice Data Center, University of Colorado, Boulder, CO.

Pail, R. *et al.*, 2011. First GOCE gravity field models derived by three different approaches, *J. Geod.,* **85**(11), 819–843.

Pattyn, F., De Smedt, B. & Souchez, R., 2004. Influence of subglacial Lake Vostok on the regional ice dynamics of the Antarctic ice sheet: a model study, *J. Glaciol.,* **50**(171), 583–589.

Petit, J. *et al.*, 1999. Climate and atmospheric history of the past 420,000 years from the Vostok ice core, Antarctica, *Nature,* **399,** 429–436.

Popov, S. & Chernoglazov, Y., 2011. Podlednikovoe ozero Vostok, Vostochnaya Antarktida: beregovaya liniya i okruzhayushchie vodoemy [Vostok Subglacial Lake, East Antarctica: lake shoreline and subglacial water caves], *Ice Snow,* **N1**(113), 12–24.

Popov, S. & Masolov, V., 2007. Forty-seven new subglacial lakes in the 0-110° E sector of East Antarctica, *J. Glaciol.,* **53**(181), 289–297.

Popov, S., Sheremetyev, A., Masolov, V., Lukin, V., Mironov, A. & Luchinin-ov, V., 2003. Velocity of radio-wave propagation in ice at Vostok station, Antarctica, *J. Glaciol.,* **49**(165), 179–183.

Popov, S., Lastochkin, A., Masolov, V. & Popkov, A., 2006. Morphology of the subglacial bed relief of Lake Vostok basin area (Central East Antarctica) based on RES and seismic data, in *Antarctica: Contribution to Global Earth Sciences,* pp. 141–146, eds Fütterer, D.K., Damaske, D., Kleinschmidt, H., Miller, H. & Tessensohn, F., Springer-Verlag.

Priscu, J. *et al.*, 1999. Geomicrobiology of subglacial ice above Lake Vostok, Antarctica, *Science,* **286,** 2141–2144.

Rémy, F., Shaeffer, P. & Legrésy, B., 1999. Ice flow physical processes derived from ERS-1 high-resolution map of the Antarctica and Greenland ice sheets, *Geophys. J. Int.,* **139,** 645–656.

Richter, A. *et al.*, 2008. Observational evidence on the stability of the hydroglaciological regime of subglacial Lake Vostok, *Geophys. Res. Lett.,* **35,** L11502.

Roemer, S., Legrésy, B., Horwath, M. & Dietrich, R., 2007. Refined analysis of radar altimetry data applied to the region of the subglacial Lake Vostok/Antarctica, *Remote Sens. Environ.,* **106,** 269–284.

Rummel, R. & Sansò, F., 1993. *Satellite Altimetry in Geodesy and Oceanography,* Lecture Notes in Earth Sciences, Vol. 50, Springer-Verlag, Berlin.

Scheinert, M., Müller, J., Dietrich, R., Damaske, D. & Damm, V., 2008. Regional geoid determination in Antarctica utilizing airborne gravity and topography data, *J. Geod.,* **82**(7), 403–414.

Schrama, E., 1989. *The Role of Orbit Errors in Processing of Satellite Altimeter Data,* Publication on Geodesy 33, Netherlands Geodetic Commission, Delft.

Schutz, B., Zwally, H., Shuman, C., Hancock, D. & DiMarzio, J., 2005. Overview of the ICESat Mission, *Geophys. Res. Lett.,* **32,** L21S01, doi:l0.1029/2005GL024009.

Shuman, C., Harding, D., Cornejo, H. & Suchdeo, V., 2011. Assessment of range bias in the ICESat (2003–2009) elevation time series and elevation changes at large subglacial lake sites, Antarctica, *Geophys. Res. Abstr.,* **13,** EGU2011–9259.

Siegert, M., Kwok, R., Mayer, C. & Hubbard, B., 2000. Water exchange between the subglacial Lake Vostok and the overlying ice sheet, *Nature,* **403,** 643–646.

Siegert, M., Ellis-Evans, J., Tranter, M., Mayer, C., Petit, J.-R., Salamatin, A. & Priscu, J., 2001. Physical, chemical and biological processes in Lake Vostok and other Antarctic subglacial lakes, *Nature,* **414,** 603–609.

Siegert, M. *et al.*, 2007. Exploration of Ellsworth subglacial lake: a concept paper on the development, organisation and execution of an experiment to explore, measure and sample the environment of a West Antarctic subglacial lake, *Rev. Environ. Sci. Biotechnol.,* **6**(1), 161–179, doi:10.1007/s11157-006-9109-9.

Siegert, M., Popov, S. & Studinger, M., 2011. Vostok subglacial lake: a review of geophysical data regarding its discovery and topographic setting, *Geophys. Monogr. Ser.,* **192,** 45–60.

Siegfried, M., Hawley, R. & Burkhart, J., 2011. High-resolution ground-based GPS measurements show intercampaign bias in ICESat elevation data near Summit, Greenland, *IEEE Trans. Geosci. Remote Sens.,* **49**(9), 3393–3400.

Smith, W. & Wessel, P., 1990. Gridding with continuous curvature splines in tension, *Geophysics,* **55,** 293–305.

Studinger, M. *et al.*, 2003. Ice cover, landscape setting, and geological framework of Lake Vostok, East Antarctica, *Earth planet. Sci. Lett.,* **205**(3–4), 195–210.

Thoma, M., Grosfeld, K. & Mayer, C., 2008. Modelling accreted ice in subglacial Lake Vostok, Antarctica, *Geophys. Res. Lett.,* **35,** L11504, doi:10.1029/2008GL033607.

Urban, T. & Schutz, B., 2005. ICESat sea level comparisons, *Geophys. Res. Lett.,* **32,** L23S10, doi:l0.1029/2005GL024306.

Vaughan, D., 1994. Investigating tidal flexure on an ice shelf using kinematic GPS, *Ann. Glaciol.,* **20,** 372–376.

Wendt, A. *et al.*, 2005. The response of the subglacial Lake Vostok, Antarctica, to tidal and atmospheric pressure forcing, *Geophys. J. Int.,* **161,** 41–49.

Wendt, J. *et al.*, 2006. Geodetic observations of ice flow velocities over the southern part of subglacial Lake Vostok, Antarctica, and their glaciological implications, *Geophys. J. Int.,* **166,** 991–998.

Williams, J., 2001. Application of a three-dimensional numerical model to Lake Vostok: an Antarctic subglacial lake, *Geophys. Res. Lett.,* **28**(3), 531–534.

Wüest, A. & Carmack, E., 2000. A priori estimates of mixing and circulation in the hard-to-reach water body of Lake Vostok, *Ocean Modelling,* **2,** 29–43.

Zwally, H. *et al.*, 2002. ICESat's laser measurements of polar ice, atmosphere, ocean, and land, *J. Geodyn.,* **34**(3–4), 405–445.

SUPPORTING INFORMATION

Additional Supporting Information may be found in the online version of this article:

Supplement. DEM of ellipsoidal ice-surface heights in the Lake Vostok region (lat: −79.5° to −75.5°, lon: 98° to 112°) derived by a regional crossover adjustment (solution S1) from ICESat laser altimeter measurements between 2003 February and 2009 October.

Please note: Wiley-Blackwell are not responsible for the content or functionality of any supporting materials supplied by the authors. Any queries (other than missing material) should be directed to the corresponding author for the article.